Journal of Materials Chemistry C

Accepted Manuscript

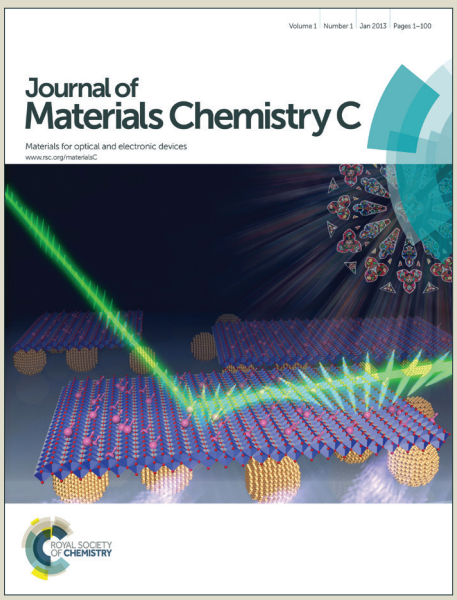

ROYAL SOCIETY OF CHEMISTRY

www.rsc.org/materialsC

ARTICLE TYPE www. rsc.org/xxxxxx | XXXXXXXX

$SrCu_3V_2O_8(OH)_2$ – dynamic Jahn-Teller distortions and orbital frustration in a new $S = \frac{1}{2}$ kagome antiferromagnet

David Boldrin[a] **and Andrew S. Wills***[a]

Received Xth XXXXXXXXXX 20XX, Accepted Xth XXXXXXXXX 20XX
First published on the web Xth XXXXXXXXXX 200X
DOI: 10.1039/b000000x

In this article we report the synthesis of a new model $S = \frac{1}{2}$ KAFM, $SrCu_3V_2O_8(OH)_2$, the Sr^{2+} analogue of vesignieite created by substitution of Ba^{2+} by isomagnetic Sr^{2+}, hereafter referred to as 'Sr-vesignieite'. Like many other kagome magnets, the magnetic moments in 'Sr-vesignieite' are hosted by Jahn-Teller distorted Cu^{2+} ions, which possess orbital degeneracy. Rather than causing a static and coherent distortion to the crystal structure, as might have been predicted, our studies of the crystallographic and bulk magnetic properties of 'Sr-vesignieite' evidence orbital fluctuations and orbital-ordering transitions. The mediating role of orbitals in superexchange leads to a natural coupling of the spin and orbital degrees-of-freedom, which introduces orbital-driven Ising-type modulations to the magnetic Hamiltonian. Further, we find the crystallographic signature of the dynamic Jahn-Teller effect in the other model KAFMs, indicating that the orbital fluctuations and phase transitions are more common than previously thought. It follows that behavior currently ascribed to the quantum behavior of spins may in part be due to spin-orbital fluctuations.

1 Introduction

Quantum spin liquids (QSLs) are exotic types of dynamical spin states that follow the rules of quantum mechanics with spin correlations defined by entaglement, rather than the breaking of time-reversal and rotational-translational symmetries that characterises conventional Néel order. Their involvement in unconventional electronic properties, such as high-T_c superconductivity and fractionalised quasi-particle excitations, has caused the search for experimental and theoretical examples to become one of the cornerstones of condensed matter science.[1–5] While QSL states are well characterised in 1-dimensional magnets, as the low-dimensionality allows quantum fluctuations to suppress conventional ordering[6,7], they are fragile in 2- and 3-dimensions as the increased connectivity naturally favors Néel order. Key requirements for the stabilisation of QSLs are the frustration of static long-ranged magnetic order and large quantum fluctuations commonly associated with the $S = \frac{1}{2}$ limit. Experimentally, the most promising model systems for exploring these states in 2-dimensions are the $S = \frac{1}{2}$ kagome Heisenberg antiferromagnets (KAFMs).

In the original models, the coupling energy between two $S = \frac{1}{2}$ moments of a Heisenberg antiferromagnet was shown to be minimised by the formation of 'valence bond' dimers, entangled singlet states. The theoretical predictions of the $S = \frac{1}{2}$ KAFMs ground state are based around configurations of these valence bonds and range from the ordered valence bond crystals (VBCs) to QSLs[8–10]. While much of the drive for chemists has historically been towards the synthesis of so-called 'perfect' KAFMs that should match well the simplified models of theory, recently there has been a growing acceptance that the perturbations present in experimental materials do not necessarily quench all aspects of frustration, and can themselves lead to exotic and interesting ground states in both the quantum and classical limits. To further understand $S = \frac{1}{2}$ KAFMs, and consequently the richness of possible QSL ground states, it is therefore important to expand the number of model materials and determine how they differ from the highly symmetric spin-only Heisenberg model.

The diverse characteristics seen in current $S = \frac{1}{2}$ KAFM model systems exemplify how frustration can survive additional energy terms and the difficulties in working out their intrinsic properties. Herbertsmithite, γ-$ZnCu_3(OH)_6Cl_2$, does not enter long-range magnetic Bragg order as $T \rightarrow 0\,K$ and shows hallmarks of QSL behaviour with a dynamic nearest-neighbour dimer ground state[4]. This is despite a significant out-of-plane Dzyaloshinskii-Moriya (DM) exchange, D_z, and Cu^{2+}/Zn^{2+} site disorder[11]. The complexity of the phase diagram of possible ground states is well exemplified by comparing herbertsmithite with its polymorph, kapellasite (α-

† Electronic Supplementary Information (ESI) available: tables of crystal data, refinement parameters and an X-ray crystallographic data file for 'Sr-vesignieite' from the synchrotron data. See DOI: 10.1039/b000000x/

[a] *Address, Department of Chemistry, University College London, 20 Gordon Street, London, UK, WC1H 0AJ.*
∗ Corresponding author.

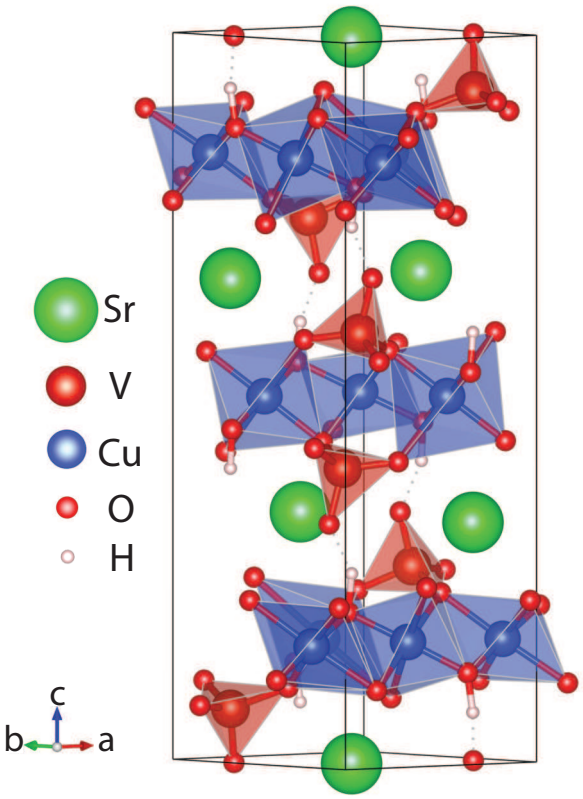

Fig. 1 Crystal structure of 'Sr-vesignieite', $SrCu_3V_2O_8(OH)_2$ at 300 K, described in space group $P3_121$ with lattice parameters $a = 5.89577(2)$ Å and $c = 20.41259(20)$ Å. The kagome layers of CuO_6 octahedra are separated by distorted 8-coordinate SrO_8 units and VO_4 tetrahedra.

$ZnCu_3(OH)_6Cl_2$)[12,13]: the two materials share the same formula and so could be expected to have similar ground-states, but instead kapellasite displays a different type of QSL that is derived from frustrated ferromagnetic and antiferromagnetic interactions. This leads to a QSL that is based on dynamic short-range correlations with the 12-sublattice cuboc2-structure.[14]. Even what should be isoelectronic and isostructural materials can behave quite differently, with only minor changes to the exchange pathways and the energy scales they mediate, causing the magnesium analogue of kapellasite, haydeeite (α-$MgCu_3(OH)_6Cl_2$), to instead possess a complex heterogenous state with coexisting long-range and short-range order below $T = 4$ K[13,15].

Some of the best model $S = \frac{1}{2}$ kagome magnets are based on copper vanadate minerals. Of particular interest is the mineral vesignieite, $BaCu_3V_2O_8(OH)_2$ which was originally proposed to crystallise with $C12/m1$ symmetry[16]. Early powder X-ray diffraction work showed that the reduction in symmetry from trigonal to monoclinic is associated with only a tiny distortion of the kagome lattice : the triangles are isosceles and have sides that differ in length by only $\sim 0.07\,\%$[17]. Consequently, it is expected to be a good realisation of the kagome geometry and its frustration causes the magnetic moments to remain disordered down to low temperatures, $T_N \approx 9$ K, well below the Weiss temperature, $\theta_w \approx -70$ K[18]. Below T_N physical properties are sample dependent, with separate evidence of both complete long-range order and an unusual state of ordered and fluctuating spins, situations that are believed to be stabilised by an in-plane DM interaction, D_p[19–21]. The importance of sample preparation and high quality structural studies of frustrated magnets is highlighed by vesignieite, with the single crystal samples being proposed to crystalise instead with the modified β-vesignieite structure in the rhombohedral space group $R\bar{3}m$[22]. Further exotic physics is shown in the closely related mineral volborthite, $Cu_3V_2O_7(OH)_2{\cdot}2H_2O$, which has been suggested to undergo a unique orbital switching transition where the lone d^9 Cu^{2+} electron moves between the $d_{x^2-y^2}$ and d_{z^2} orbitals as a function of temperature[23]. We will return to this hypothesis and the structure of vesignieite later in this article.

Here we report the synthesis and initial characterisation of a new model $S = \frac{1}{2}$ KAFM, $SrCu_3V_2O_8(OH)_2$, hereafter referred to as 'Sr-vesignieite'. Whilst this material shares many structural features with the isomagnetic barium-based vesignieite, such as Cu^{2+} kagome layers separated by VO_4 tetrahedra and group 2 ions (Ba^{2+}/Sr^{2+}) (Figure 1), it does not crystallise in either of the $C12/m1$ or $R\bar{3}m$ space groups proposed for vesignieite, but rather is best described in the trigonal space group $P3_121$. The kagome lattice in this structure features a distorted geometry with two crystallographically inequivalent CuO_6 octahedra that at high temperature have local geometries consistent with dynamic Jahn-Teller (JT) fluctuations of the $d_{x^2-y^2}$ orbitals that mediate the magnetic exchange interactions. Upon cooling, one of the Cu sites enters an antiferro-orbital ordered state but the other continues to fluctuate, causing the kagome network to be decorated with a triangular geometry of dynamical orbitals. Spin frustration coexists with the orbital fluctuations over a wide temperature range, as evidenced by a highly suppressed magnetic transition ($\frac{|\theta_W|}{T_N} \sim 9$) with respect to the first Jahn-Teller orbital-ordering temperature of $T_{JT} \sim 230$ K. These phenomena are reminiscent of the spin-orbital liquids $FeSc_2S_4$[24] and $Ba_3CuSb_2O_9$[25,26] where the JT-active Fe^{3+} and Cu^{2+}, respectively, do not undergo cooperative JT distortions as both their orbitals and spins are highly frustrated. Furthermore, we show that crystallographic data of several closely related $S = \frac{1}{2}$ KAFMs are also compatible with the dynamic JT effect, which raises the need to re-evaluate more generally the role orbitals play in orbitally degenerate frustrated magnets.

2 Experimental

Inspiration for the synthesis of 'Sr-vesignieite' was taken from similarities between the layered crystal structures of volborthite, $Cu_3V_2O_7(OH)_2.2H_2O$, and 'Sr-vesignieite': volborthite and vesignieite are built from kagome layers of Cu^{2+} interspaced by V_2O_7/H_2O and VO_4/Sr^{2+} groups, respectively. Under hydrothermal conditions it was found that volborthite could be converted into 'Sr-vesignieite' through substitution of Sr^{2+} for the H_2O group and reaction of $V_2O_7^{4-}$ groups to form VO_4^{3-}. Precipitation of the unwanted side product, $SrCuVO_4(OH)$, was minimised by using an acidified solution and grinding the volborthite starting material to form a homogenously powdered sample.

The final preparation conditions for 'Sr-vesignieite' were as follows. Powdered volborthite (200 mg, 0.4214 mmol) was lightly ground for ~1 min and added to a 20 ml PTFE reaction vessel along with $Sr(CH_3COO)_2$ (90.5 mg, 0.4214 mmol) and H_2O (10 ml). The solution was stirred for 2 mins before being sealed in a steel autoclave and placed in an oven at 220 °C for 2 days. The autoclave was left to cool to room temperature before the product was collected and centrifuged in water. The top, green coloured layer was collected and washed with water and acetone before being dried on a rotary evaporator. The resulting product was found to be phase pure and highly crystalline according to the following powder X-ray diffraction (XRD) analysis and the final yield was ≈ 80 mg (35 %).

3 Results and Discussion

Synchrotron data was collected from a powdered sample of 'Sr-vesignieite' on the 11-BM beamline at the Advanced Photon Source (APS) at room temperature using X-rays of wavelength $\lambda = 0.413827$ Å. Indexing and refinements were performed using the TOPAS software[27]. Initial investigations indicated that the monoclinic, $C12/m1$, structure originally suggested for vesignieite could not account for all of the reflections present and instead the pattern was found to index with the trigonal $P3_1$ space group (Figure 2 inset). Pawley refinement using this structure gave an excellent fit with lattice parameters $a = 5.89577(2)$ Å and $c = 20.41259(20)$ Å. A noticeable *hkl*-dependent peak broadening arising from out of register layers was modelled using Stephens's approach and an additional circles convolution ($1 - \left|\frac{\varepsilon_m}{\varepsilon}\right|^2$ for $0 \leq \varepsilon \leq \varepsilon_m$) was applied to model the asymmetry of the 00*l* reflections[28]. We note that the sample contribution to peak broadening is both smaller and less complex than for our vesignieite samples prepared *via* a reflux method[17], demonstrating that 'Sr-vesignieite' features better sample crystallinity.

With several space groups allowing the same reflection conditions as $P3_1$, further analysis of the diffraction pattern was

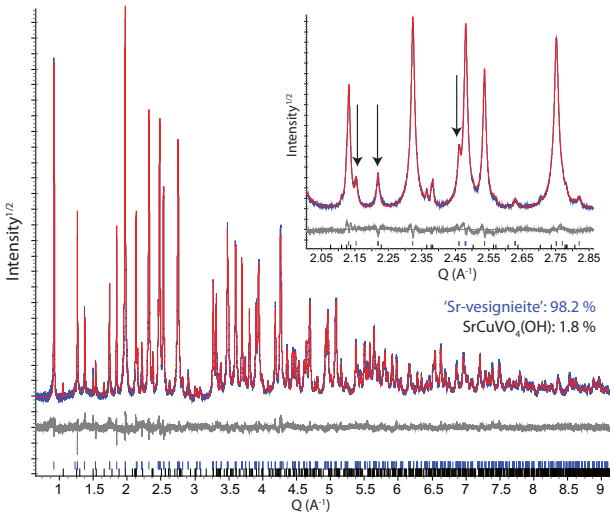

Fig. 2 Rietveld refinement of synchrotron data measured on a powdered sample of 'Sr-vesignieite' at a wavelength of $\lambda = 0.413827$ Å. **Inset.** Expanded region of the plot. Arrows indicate peaks which are not accounted for by the $C12/m1$ structure but instead index and are correctly refined with a $P3_121$ structure. The final goodness-of-fit parameters were $\chi^2 = 1.413$ and $R_{wp} = 6.878$ for 71 variables.

performed using the minimal supergroups of $P3_1$ that retained appropriate Wyckoff site degeneracies, namely $P3$, $R3$, $P3_112$, $P3_121$ and $P6_4$. Relevant crystallographic transformations were calculated using the program PSEUDO[29]. $P3$ and $R3$ could be immediately excluded as possible symmetries as they failed to index the observed reflections, whilst $P3_112$ and $P6_4$ required unphysically large displacements (> 2 Å) of atoms from the original monoclinic vesignieite structure. $P3_121$ was found to correctly index the observed reflections and gave atomic positions that agreed well with the vesignieite structure. After completing Rietveld analysis in $P3_121$, lowering the symmetry of the refinement to $P3_1$ was tested and found to not significantly improve the quality of the fit. The final Rietveld refinement to the synchrotron data was therefore completed in $P3_121$ and the calculated and experimental profiles are presented in Figure 2a ($\chi^2 = 1.511$ for 71 variables).

According to the trigonal $P3_121$ structure, the kagome lattice of 'Sr-vesignieite' is constructed from two crystallographically inequivalent Cu^{2+} sites (Figure 3a): the Cu1 sites form chains along the [110] direction which are connected by Cu2 sites. We note that the Cu2 sites themselves form a larger triangular network that is capable of supporting geometric frustration. A consequence of the symmetry of the $P3_121$ space group is that the individual triangles of the kagome are scalene rather than isosceles or equilateral, and have 3 inequivalent sides of 2.936(2), 2.948(2) and 2.961(2) Å. The difference between the longest and shortest Cu–Cu bond lengths is

very small, ~ 0.8 %, and so 'Sr-vesignieite' can be considered metrically as a pseudo-perfect $S = \frac{1}{2}$ KAFM. We further suggest that the small nature of the distortion prevously seen in powder samples of synthetic barium vesignieite[13] would make incorrect assignment of the space group a possibility that is strengthened by the poor crystallinity of some samples and recommend reinvestigation of vesignieite in terms of the $P3_121$ structure found here for 'Sr-vesignieite'.

We look now in detail at the local co-ordination environments of the two Cu^{2+} sites at room temperature. The Cu2 site is remarkable as the refined structure features four long and two short Cu–O bonds (Figure 3b), *i.e.* the site appears to involve an *axially compressed* JT distortion. This is of interest as the vast majority of static Cu^{2+} JT distortions involve axial elongation due to preferential filling of the d_{z^2} orbital. *Axial compression* in structures derived from powder diffraction data needs to be treated with suspicion as it has been shown that it can be an average structure that results from the time-averaging of fluctuations between two degenerate co-ordination configurations in which the *axial elongations* point along different directions[32]. This situation is represented in Figure 3c.

In $P3_121$ the co-ordination of the Cu1 site appears to be a distorted octahedron that is made up of three pairs of Cu–O bond lengths, with each pair of bonds lying oppositely around the central Cu^{2+} (Figure 3b). This configuration corresponds to a *rhombically* distorted octahedron, and is another good indication of a dynamic JT effect, this time involving the average of fluctuations between two non-degenerate axially elongated geometries aligned along different Cu–O bonds (Figure 3d).[32] The refinement of the averaged structure suggests that the Cu1–O11 and Cu1–O13 bonds are significantly shorter than the equivalent bonds of Cu2. This indicates that the $d_{x^2-y^2}$ orbital of the $Cu1O_6$ octahedron spends the majority of the time aligned along these bonds, drawing these oxygens in towards Cu1.

Temperature dependent X-ray diffraction can reveal dynamic structural features and orbital ordering processes that could otherwise remain hidden by the diffraction averaging process. Using a STOE Stadi-P diffractometer equipped with a Dectris Mythen 1K detector and an Oxford Instruments CryoJetHT, X-ray diffraction spectra were collected on the same sample as before at temperatures between 105 and 400 K. Cu $k_{\alpha 1}$ radiation was used and the sample was loaded in a 0.2 mm diameter capillary so that absorption effects were small enough to negate the need for corrections. Rietveld refinements were performed using the TOPAS software.

On cooling, there is a distinct change in behaviour in the c/a lattice parameter ratio below $T_{JT} \approx 200$ K (Figure 4a). Such a feature often indicates a structural transition and is accompanied by a symmetry change, however no extra peaks or peak splittings are observed in our diffraction data below T_{JT}.

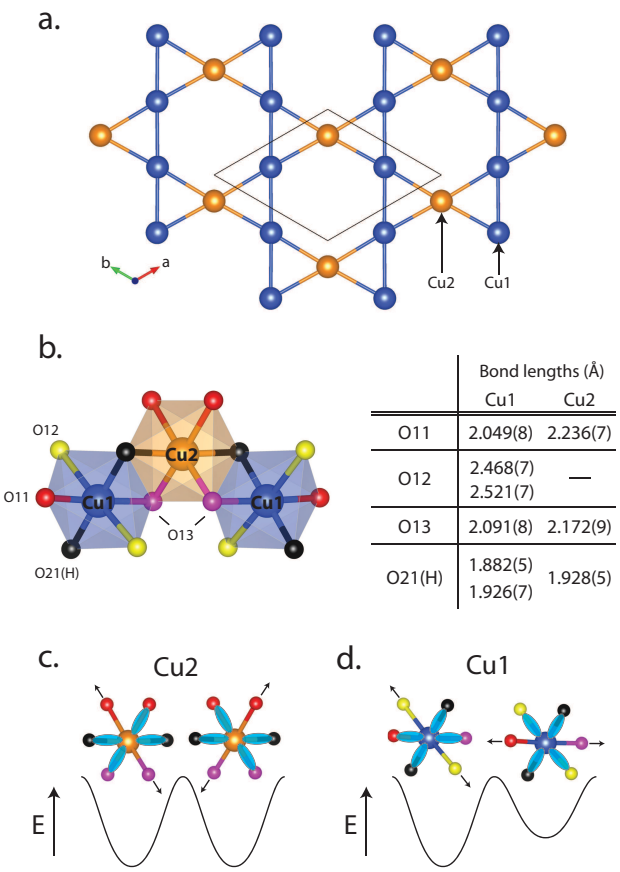

	Bond lengths (Å) Cu1	Cu2
O11	2.049(8)	2.236(7)
O12	2.468(7) 2.521(7)	—
O13	2.091(8)	2.172(9)
O21(H)	1.882(5) 1.926(7)	1.928(5)

Fig. 3 a. The kagome lattice in 'Sr-vesignieite' is built from two crystallographically inequivalent Cu^{2+}. The Cu1 sites form chains along the [110] direction whilst the Cu2 sites decorate the kagome network with a triangular sublattice. **b.** At room temperature the $Cu1O_6$ and $Cu2O_6$ octahedra are rhombically distorted and axially compressed, respectively. These distortions are indicative of dynamic JT fluctuations. **c.** The axially compressed octahedra on the Cu2 site indicates dynamic fluctuations between two states of equal energy. **d.** The rhombically distorted $Cu1O_6$ octahedra suggests a dynamic JT distortion between two states that have different energies. The bond valence sums for the Cu1 and Cu2 coordination geometries of 2.06 and 2.12, respectively[30,31], suggest that the sites are not unusual and appear not to provide clear evidence for dynamic distortions, but care should be taken in deciding how much weight to put on their interpretation as the technique fails for Jahn-Teller ions and structures used for the calculations are averages of fluctuating bonds.

We explored the possibility of a distortion below 230 K from $P3_121$ to a space group with the same *hkl* conditions by refining using $P3_1$ symmetry. This did not improve the quality of the fit, but instead destabilised the oxygen positions. We conclude therefore that within the limits of our data the transition at T_{JT} does not involve a change in space group symmetry.

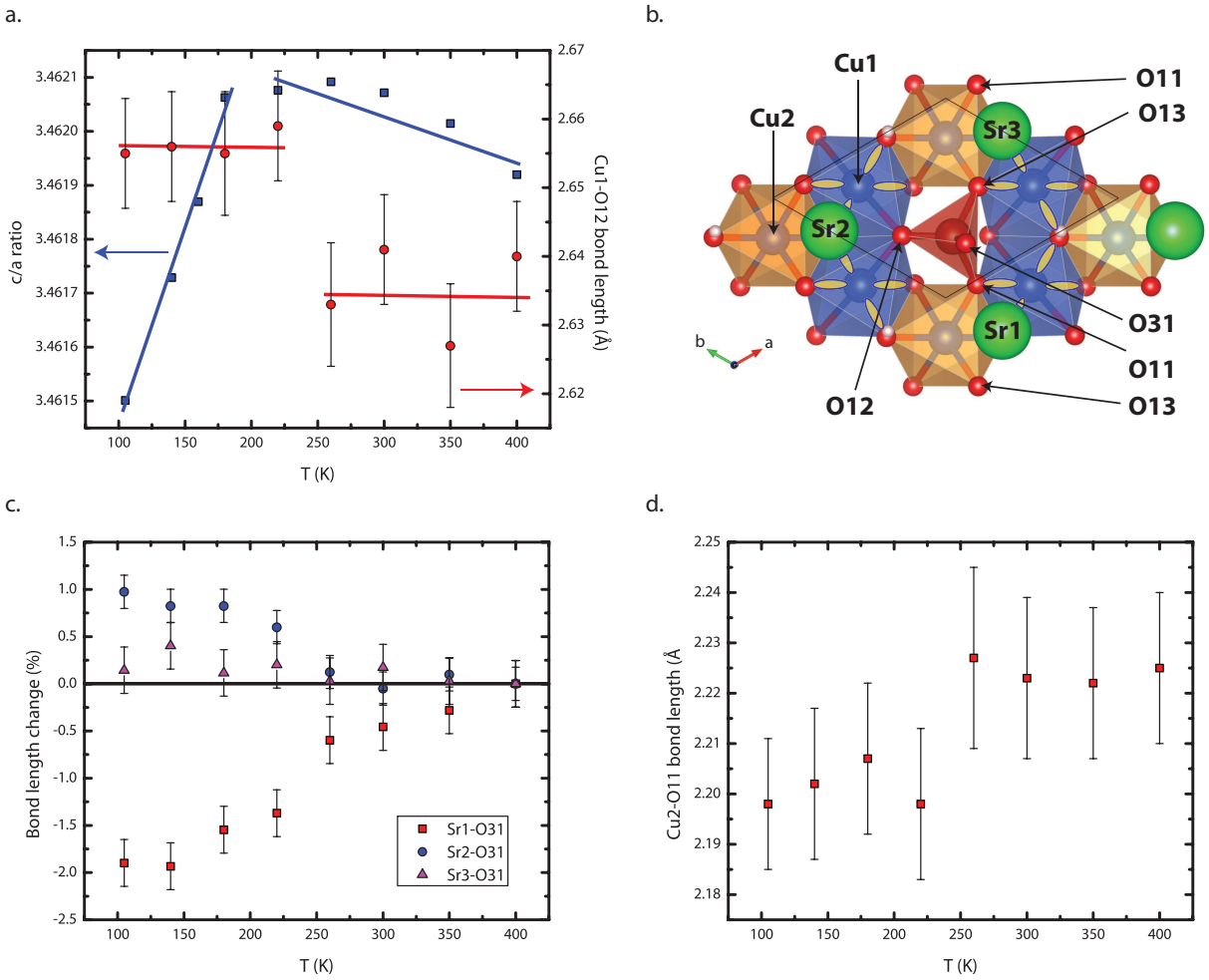

Fig. 4 a. The temperature dependence of the *c*/*a* lattice parameter ratio and Cu1–O12 bond length obtained from Rietveld refinement of X-ray diffraction data. A change in behaviour of *c*/*a* at $T_{JT} \approx 230$ K coincides with an abrupt elongation of the Cu1–O12 bond, signalling a cooperative JT distortion on the Cu1 sites. **b.** A view of a kagome plane along the [001] direction. At T_{JT} the O31 atom shifts towards Sr1, as shown in **c**, due to rotation of the VO_4 caused by the cooperative JT. The JT distortion aligns the Cu1 $d_{x^2-y^2}$ as shown.

The change in c/a at T_{JT} (Figure 4a) is accompanied by a sudden increase of the Cu1–O12 bond length. This increases the rhombic distortion of the $Cu1O_6$ octahedra and is accommodated within the structure by a simultaneous rotation of the VO_4 tetrahedra. The VO_4 rotation can be parameterised by the position of the apical O31 oxygen within the plane of Sr^{2+} ions, as shown in Figure 4b. At T_{JT}, the percentage bond length change of Sr–O31, shown in Figure 4c, indicates an abrupt shift of the O31 consistent with a rotation of the VO_4. We suggest that the cause of this transition is a co-operative JT distortion of the $Cu1O_6$ chains along the [110] direction.

Analysis of the temperature-dependent diffraction data indicates that the four longer bonds of the $Cu2O_6$ octahedra, involving the bond pairs for Cu2–O11 and Cu2–O13, are found to shorten as the temperature is decreased. While Cu2–O13 shows only a gradual shortening upon cooling, there is an abrupt change in Cu2–O11 (Figure 4d) which we conclude is characteristic of the tilting of the VO_4 units introduced above rather than a static JT distortion, as the latter would require *elongation* of one of these bonds and a lowering of both the space group $P3_121$ symmetry and the local Cu2 C_2 site symmetry. To confirm the absence of a static JT we performed refinements where the O11 and O13 sites were duplicated, with each position set to half occupancy, and their positions allowed to refine freely. This did not improve the quality of the fit and again failed to reveal any bond elongation. We thus conclude that the orbitals in Cu2 site remain dynamic due to presence of degenerate configurations below T_{JT}, a property that can be considered in terms of effective exchange interactions between orbitals as being a result of frustration[33]. At this

point we can only speculate that this degeneracy will be broken at lower temperatures and orbital ordering will occur, and look towards the results from future low temperature neutron diffraction experiements for insight.

a.

Path #	Cu1-Cu1	Angle	Path #	Cu1-Cu2	Angle
2	∠Cu1-O12-Cu1	72.1(1)°	5	∠Cu1-O11-Cu2	85.6(2)°
1	∠Cu1-O21-Cu1	104.4(2)°	4	∠Cu1-O13-Cu2	87.8(2)°
			3	∠Cu1-O21-Cu2	103.6(2)° 100.3(2)°

b.

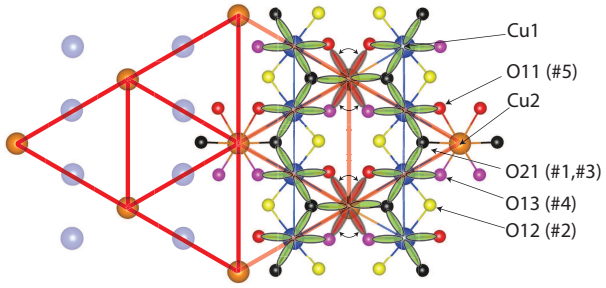

Fig. 5 a. Cu–O–Cu bond angles of the possible superexchange pathways in 'Sr-vesignieite'. **b.** Cu^{2+} $d_{x^2-y^2}$ orbital arrangements for the Cu1 (blue) and Cu2 (orange) sites. The Cu2 site fluctuates between two degenerate orbital arrangements, leaving all oxygens available to mediate superexchange with neighbouring Cu1. These dynamic Cu2 decorate the kagome network with a triangular sublattice. On the Cu1 site, below T_{JT} the $d_{x^2-y^2}$ orbitals enter a long-range antiferro-orbital ordered state with lobes aligned towards the O11, O13 and two O21(H) oxygens. The bridging atoms involved in the different superexchange pathways are indicated.

Anisotropic displacement parameters are a good indication of disordered structural features and so can be used to provide further evidence for dynamic JT distortions. Unfortunately, refinement of these parameters with our data was unstable and so we restrict ourselves to a discussion of the crystallographic analyses of the closely related material vesignieite, $BaCu_3V_2O_8(OH)_2$. There has been some controversy over the crystal structure of vesignieite with the initial single crystal XRD studies of natural vesignieite identifying the space group as $C2/m$ [16], while more recent analyses of synthetic single crystals led to the suggestions that highly crystalline vesignieite samples instead crystallise in the rhombohedral space group $R\bar{3}m$ [22]. Despite the differences in the refined structures, both works concluded that there are large anisotropic displacement parameters of the equatorial Cu–O oxygens and small, roughly spherical displacement parameters of axial Cu–O(H) bonds, and so are consistent with our picture of juxtaposed fluctuating and static orbitals.

It is clear that the nature of JT distortions in materials with orbitally degenerate Cu^{2+} ions should be considered more generally by researchers in the field. We believe that a key feature which supports the dynamic JT effect in these materials is a non-symmetry breaking tilting of the MO_4 tetrahedra (M = As or V) that is allowed when the coordination of the apical oxygen of the MO_4 is weak; this feature is present in 'Sr-vesignieite' as the O31 is only hydrogen bonded to a hydroxide group and weakly bonded to the Sr^{2+} (Sr–O31 = 2.836(5) Å). This naturally expands our discussion to the dynamic JT distortions that have already been predicted in other kagome magnets based on Cu^{2+} vanadate and arsenate minerals which, we note, have remarkably similar CuO_6 geometries to those we have described for 'Sr-vesignieite' [32]. Partial orbital ordering also appears to be present in bayldonite, $PbCu_3As_2O_8(OH)_2$, where the Cu(2)O_6 octahedron is rhombically distorted and its ligated oxygens have anisotropic displacement parameters consistent with dynamic fluctuations. The other two inequivalent CuO_6 are axially *elongated* and their anisotropic displacements do not indicate that the Cu–O bonds are dynamic. Even the well known kagome magnet volborthite, $Cu_3V_2O_7(OH)_2{\cdot}2H_2O$, and the closely related arsenate $KCu_3As_2O_7(OH)_3$ have been determined to have structures with both axially compressed and rhombically distorted CuO_6 octahedra, and anisotropic displacements that are compatible with dynamic JT fluctuations [32,34].

Looking now to the magnetism of these materials, the presence of dynamic JT distortions is important as it clarifies which orbitals mediate the magnetic superexchange interactions and whether they act as a fluctuating energy scale. If 'Sr-vesignieite' had the structure originally proposed for vesignieite itself, which had $C2/m$ symmetry and featured static JT distortions with 2 axially compressed Cu–O bonds, then we would expect the d_{z^2} Cu^{2+} orbitals to mediate the superexchange, as Okamato and coworkers concluded [18]. However, if the situation involves fluctuating, axially *elongated* distortions, the orbital arrangement instead involves the unpaired electron of Cu^{2+} being in the $d_{x^2-y^2}$ orbital. This would then allow the superexchange between nearest-neighbour Cu^{2+} to occur through multiple routes: the information about the various Cu–O–Cu superexchange pathways is listed in Figure 5a. For simplification, these paths can be split into two groups: (i) paths involving the μ_3-hydroxide group, O21(H), which coordinates with the three Cu^{2+} that constitute the kagome triangles, with bond angles $90° < \angle$Cu–O21(H)–Cu $< 104°$, and (ii) paths involving the μ_4-O11, -O12 and -O13 oxygens, which coordinate with $2\times Cu^{2+}$ in addition to the V^{5+} and Sr^{2+} ions, and have bond angles $\angle$Cu–O–Cu $< 90°$. According to the Goodenough-Kanamori rules [35], superexchange mediated along paths with angles of 90° is expected to be weakly ferromagnetic, which we can therefore attribute to the paths

involving O11, O12 and O13. By comparison with other cuprates[36–38], we can expect the superexchange mediated by the μ_3-O21(H) to be antiferromagnetic and of the order of 10 meV (~ 100 K).

Using the information concerning the superexchange paths and orbital arrangements we can begin to build a model of the magnetic interactions within the kagome lattice of 'Sr-vesignieite'. Firstly, we will concentrate on the Cu1 site. The rhombic distortion of the local coordination on this site and the cooperative JT distortion at T_{JT} indicates that the partially occupied $d_{x^2-y^2}$ orbital align towards the Cu1–O11, Cu1–O13 and two Cu1–O21(H) oxygens, forming an antiferro-orbital configuration along the Cu1 chains (Figure 5b). Therefore, the superexchange mediated by these bonds could be ferromagnetic or antiferromagnetic depending on which is chosen. On the Cu2 site, both degenerate arrangements of the $d_{x^2-y^2}$ have overlap with the O21(H) oxygen, whilst two lobes fluctuate between the remaining four O11 and O13 oxygens. This leaves all oxygens ligated to Cu2 available for superexchange with Cu1 and the potential for multiple, competing exchange interactions of both antiferromagnetic and ferromagnetic nature.

The orbitally frustrated Cu2 sites can be considered as decorating the kagome network with a triangular superlattice of Ising-like orbital degrees-of-freedom (Figure 5b). This is reminiscent of the triangular Ni^{2+} lattice in the orbital liquid $LiNiO_2$[39], which does not show any sign of co-operative JT distortions acording to X-ray diffraction data. Whilst spin and orbital frustration on the geometrically frustrated triangular lattice has been predicted to host various liquid-like ground states[40,41], this does not happen in $LiNiO_2$ as the spins and d_{z^2} orbitals are effectively decoupled due to the 90° Ni–O–Ni superexchange path[42]. In contrast, the multiple exchange paths in 'Sr-vesignieite' vary between $\sim 90°$ to $\sim 100°$, suggesting that the interplay between spin and orbital frustration will be significant.

The description in 'Sr-vesignieite' of competing antiferromagnetic and ferromagnetic exchange with both spin and orbital contributions agrees well with the magnetic susceptibility data shown in Figure 6. Taken using a Quantum Design MPMS-7 DC-SQUID magnetometer in measuring fields of 100 Oe between 2 K and 300 K, the plot of χ *vs.* T reveals a broad transition at $T_N \simeq 11$ K with associated separation of zero-field-cooled (ZFC) and field-cooled (FC) data (Figure 6a). Re-plotting the data as χT *vs.* T reveals a peak at T_N on top of the general downwards trend (Figure 6b) and a magnetic behaviour that is close to that seen for vesignieite itself. A fit to the χ^{-1} *vs.* T to the Curie-Weiss law over the temperature range 150 K to 300 K yielded a Weiss temperature, $\theta_w = -100 \pm 5$ K, demonstrating that the net exchange remains strongly antiferromagnetic and that the magnetic transition is suppressed (Figure 6c) with respect to this mean field. For comparison, Figure 6b also shows data collected from the barium-analogue, vesignieite itself, with the inset showing the derivative $d\chi/dT$. The magnetic properties of these iso-magnetic materials feature similar values of T_N, it is only 2 K lower in 'Sr-vesignieite', and although the transition is less well defined in this sample of barium vesignieite, the derivatives $d\chi T/dT$ are comparible. Other samples of vesignieite with improved crystallinity exhibit a comparably sharp transition[19,22] to that of 'Sr-vesignieite'. The observation of magnetic field-dependent hysteresis below this transition in vesignieite confirms the presence of competing exchange interactions and magnetic frustration that we expect also to be present in 'Sr-vesignieite'. The larger magnitude of χ_{FC} as $T \to 0$ K suggests that it possesses a larger ferromagnetic component than its barium based relative, vesignieite.

Looking now at the higher temperature behaviour, at first glance, χ^{-1} *vs.* T closely follows Curie-Weiss behaviour above $T \approx 100$ K, however upon closer inspection, a slight change in gradient occurs at $T \approx 210$ K, *i.e.* in the region of T_{JT} (Figure 6d). Fits to the linear regions $100 < T < 190$ K and $230 < T < 300$ K yield different Weiss temperatures and Curie constants: $\theta_w = -112$ K and $C = 0.530$ emu K mol^{-1} in the low temperature region and $\theta_w = -92$ K and $C = 0.498$ emu K mol^{-1} at higher temperature. Using the same fitting procedure for several 50 K regions between 300 and 100 K, the calculated effective moment, μ_{eff}, is found to increase upon cooling before plateauing at T_{JT} (Figure 6d inset). The larger than expected μ_{eff} ($\mu_{spin-only} = 1.73\,\mu_B$) is most likely a consequence of an enhanced Landé g-factor due to an orbital contribution, as is commonly observed in Cu^{2+} ions – similar enhancement of μ_{eff} at the orbital ordering transition is observed in the material Ag_2NiO_2[43]. Furthermore, the concomitant increase in the magnitude of the antiferromagnetic Weiss temeprature θ_w on cooling below T_{JT} is consistent with the transiton being to antiferro-orbital order, as depicted in Figure 5b.

4 Conclusion

In conclusion, we have synthesised a new model $S = \frac{1}{2}$ kagome magnet, 'Sr-vesignieite' - $SrCu_3V_2O_8(OH)_2$, that is isomagnetic with the barium-based mineral vesignieite and crystallises in the space group $P3_121$. Magnetisation data indicate that there is long-range magnetic order below $T_N \simeq 11$ K and that the transiton is suppressed by magnetic frustration.

Synchrotron and laboratory powder X-ray diffraction data reveal that the crystal structure of 'Sr-vesignieite' should not be considered 'passive' but that there are instead dynamic JT distortions of two types: those of the Cu1 octahedra involve fluctuations between non-degenerate orbital configurations which freeze out at $T_{JT} \approx 230$ K; those of the Cu2 octahedra are between two degenerate orbital configurations and

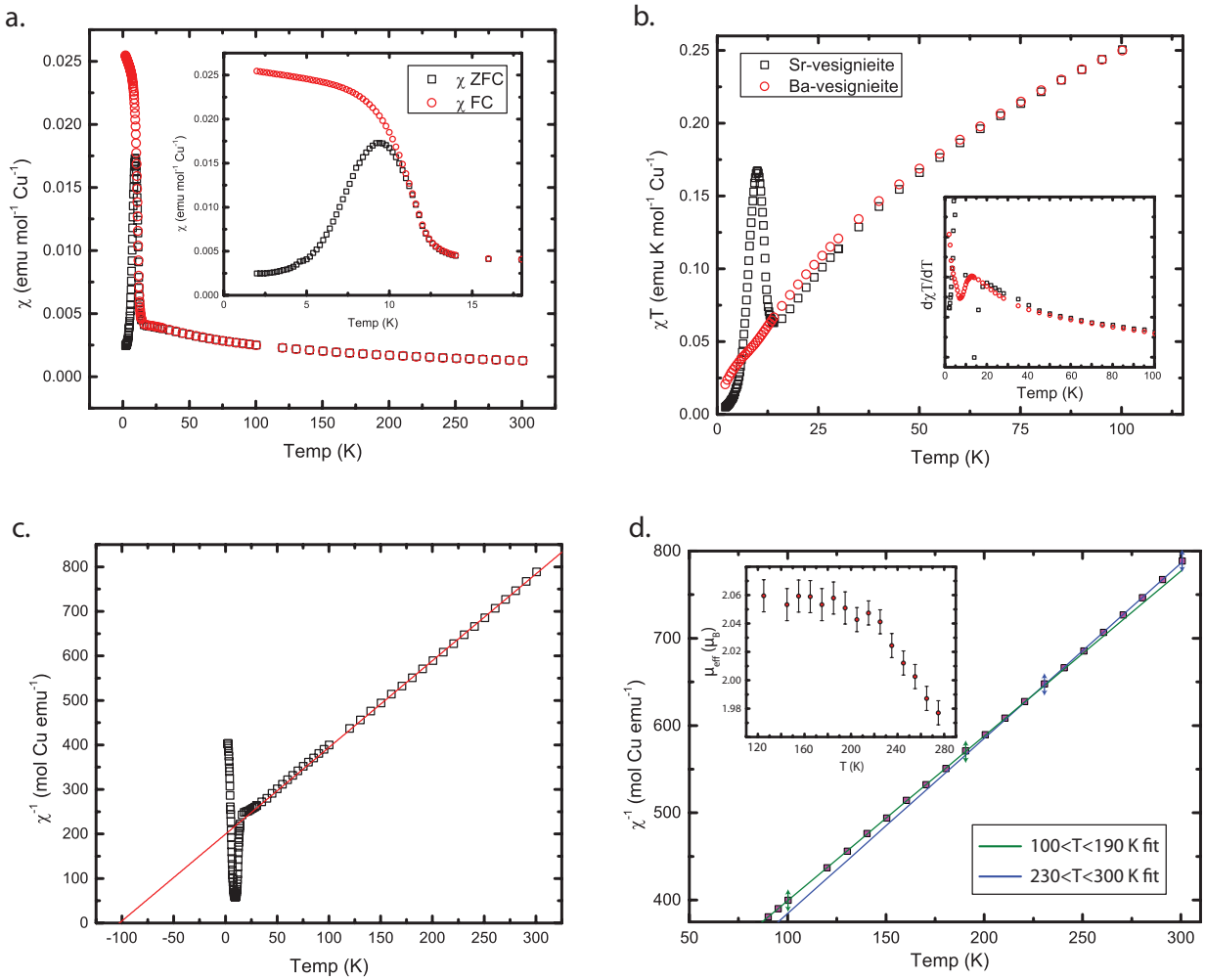

Fig. 6 a. A plot of zero-field cooled and field cooled χ *vs*. T measured at 100 Oe. The inset shows a zoom in on the transition at $T_N = 11$ K. **b.** A comparison of the T-dependence of χT for vesignieite and 'Sr-vesignieite'. Whilst the low-T transition is more prominent in 'Sr-vesignieite', the derivatives (**inset**) show very similar behaviour. **c.** A plot of χ^{-1} *vs*. T. A fit to the $150 \leq T \leq 300$ K region, indicated by the black line, gives a Curie-Weiss temperature of $\theta_w = -100 \pm 5$ K demonstrating strong antiferromagnetic interactions. **d.** A change in gradient of χ^{-1} at high temperature coincides with the orbital ordering transition at T_{JT}. The more negative θ_w below T_{JT} is consistent with the predicted antiferro-orbital order and the fitted values of μ_{eff} plateaus at $\sim T_{JT}$ (**inset**).

there is no evidence of them freezing down to 105 K. The Cu2 $d_{x^2-y^2}$ orbitals therefore act as an Ising-like degree-of-freedom that will couple through the superexchange parameters to the frustrated spin system. The combination of frustrated spin and orbital degrees of freedom in 'Sr-vesignieite' makes it a candidate for exploring quantum spin-orbital ground states.

Our analysis also indicates the possibility of related dynamic orbital configurations in other model quantum kagome materials and consequently raises the question of how its effects manifest themselves in the observed magnetism and phase transitions of this group of materials. We suggest that dynamic Jahn-Teller distortions and orbital ordering transitions provide an alternative explanation for the orbital switching proposed to occur in volborthite[23].

References

1 Anderson, P. W. *Science* **1978**, *201*, 307–16
2 Balents, L. *Nature* **2010**, *464*, 199–208
3 de Vries, M. A.; Stewart, J. R.; Deen, P., P.; Piatek, J., O.;Nilsen, G. J.; Rønnow, H., M.; Harrison, A. *Phys. Rev. Lett* **2009**, *103*, 237201
4 Han, T.-H.; Helton, J. S.; Chu, S.; Nocera, D. G.; Rodriguez-Rivera, J. A.; Broholm, C.; Lee, Y. S. *Nature* **2012**, *492*, 406–410
5 Sachdev, S. *Nat. Phys.* **2008**, *4*, 173–185
6 Zaliznyak, I. A.; Woo, H.; Perring, T. G.; Broholm, C. L.; Frost, C. D.; Takagi, H. *Phys. Rev. Lett.* **2004**, *93*, 087202

7 Mourigal, M.; Enderle, M.; Klöpperpieper, A.; Caux, J.-S.; Stunault, A.; Rønnow, H. M. *Nat. Phys.* **2013**, *9*, 435–441
8 Lacroix, C.; Mendels, P.; Mila, F. *Introduction to Frustrated Magnetism*; Springer-Verlag: Berlin, 2011
9 Singh, R. R. P. *Phys. Rev. B* **2007**, *76*, 180407
10 Hermele, M.; Ran, Y.; Lee, P.; Wen, X.-G. *Phys. Rev. B* **2008**, *77*, 224413
11 Zorko, A.; Nellutla, S.; van Tol, J.; Brunel, L.; Bert, F.; Duc, F.; Trombe, J.-C.; de Vries, M.; Harrison, A.; Mendels, P. *Phys. Rev. Lett.* **2008**, *101*, 25–28
12 Colman, R.; Ritter, C.; Wills, A. S. *Chem. Mater.* **2008**, *20*, 6897
13 Colman, R.; Sinclair, A.; Wills, A. S. *Chem. Mater.* **2010**, *22*, 5774–5779
14 Fåk, B.; Kermarrec, E.; Messio, L.; Bernu, B.; Lhuillier, C.; Bert, F.; Mendels, P.; Koteswararao, B.; Bouquet, F.; Ollivier, J.; Hillier, A. D.; Amato, A.; Colman, R. H.; Wills, A. S. *Phys. Rev. Lett.* **2012**, *109*, 037208
15 Kermarrec, E. *Nouveaux états quantiques de spin induits par frustration magnétique sur le réseau kagome*. Ph.D. thesis, 2012
16 Zhesheng, M.; Ruilin, H.; Xiaoling, Z. *Acta Geol. Sin.-Engl.* **1991**, *4*
17 Colman, R.; Bert, F.;Boldrin, D.; Hillier, A.; Manuel, P.; Wills, A. S. *Phys. Rev. B.* **2011**, *18*, 180416
18 Okamoto, Y.; Yoshida, H.; Hiroi, Z. *J. Phys. Soc. Jpn* **2009**, *78*, 033701
19 Yoshida, M.; Okamoto, Y.; Yoshida, H. *J. Phys. Soc. Jpn* **2013**, *82*, 013702
20 Quilliam, J.; Bert, F.; Colman, R.; Boldrin, D.; Wills, A. S.; Mendels, P. *Phys. Rev. B* **2011**, *84*, 180401
21 Zorko, A.; Bert, F.; Ozarowski, A.; van Tol, J.; Boldrin, D.; Wills, A. S.; Mendels, P. *Phys. Rev. B* **2013**, *88*, 144419
22 Yoshida, H.; Michiue, Y.; Takayama-Muromachi, E.; Isobe, M. *J. Mater. Chem.* **2012**, *22*, 18793
23 Yoshida, H.; Yamaura, J.-I.; Isobe, M.; Okamoto, Y.; Nilsen, G. r. J.; Hiroi, Z. *Nat. Comm.* **2012**, *3*, 860
24 Krimmel, A.; Mücksch, M.; Tsurkan, V.; Koza, M.; Mutka, H.; Loidl, A. *Phys. Rev. Lett.* **2005**, *94*, 237402
25 Ishiguro, Y.; Kimura, K.; Nakatsuji, S.; Tsutsui, S.; Baron, A. Q. R.; Kimura, T.; Wakabayashi, Y. *Nat. Comm.* **2013**, *4*, 2022
26 Shanavas, K. V.; Popović, Z. S.; Satpathy, S. *Phys. Rev. B* **2014**, *89*, 085130
27 Bruker AXS, TOPAS V4: General profile and structure analysis software for powder diffraction data. 2008
28 Stephens, P. W. *J. Appl. Crystallogr.* **1999**, *32*, 281–289
29 Capillas, C.; Tasci, E.; de la Flor, G.; Orobengoa, D.; Perez-Mato, J.; Aroyo, M. *Z. Kristallogr.* **2011**, *226*, 186–196
30 O'Keeffe, M., *Structure and Bonding* (1989),*71*, 161–190
31 Wills, A. S. *VaList*, Program available from www.ccp14.ac.uk
32 Burns, P.; Hawthorne, F. *Can. Mineral* **1996**, *34*, 1089–1105
33 Khomskii, D. I.; Mostovoy, M. V. *J. Phys. A: Math. Gen.* **2003**, *36*, 9197.
34 Okamoto, Y.; Ishikawa, H.; Nilsen, G. J.; Hiroi, Z. *J. Phys. Soc. Jpn* **2012**, *81*, 033707
35 Goodenough, J. B. *Physical Review* **1955**, *100* 564. Goodenough, J. B. *Journal of Physics and Chemistry of Solids* **1958**, *6* 287. Kanamori J., *J. Phys. Chem. Solids* **1959**, *10* 87
36 Rocquefelte, X.; Schwarz, K.; Blaha, P. *Scientific Reports* **2012**, *2*, 759
37 Mizuno, Y.; Tohyama, T.; Maekawa, S. *Phys. Rev. B* **1998**, *57*, 5326–5335
38 Wills, A. S. and Henry, J.-Y. *J. Phys.: Condens. Matter* **2008**, *20*, 472206
39 Reynaud, F.; Mertz, D.; Celestini, F.; Debierre, J.-M.; Ghorayeb, A. M.; Simon, P.; Stepanov, A.; Voiron, J.; Delmas, C. *Phys. Rev. Lett.* **2001**, *86*, 3638–3641
40 Penc, K.; Mambrini, M.; Fazekas, P.; Mila, F. *Phys. Rev. B* **2003**, *68*, 012408
41 Mila, F.; Vernay, F.; Ralko, A.; Becca, F.; Fazekas, P.; Penc, K. *J. Phys.-Condens. Mat.* **2007**, *19*, 145201
42 Mostovoy, M. V; Khomskii, D. I. *Phys. Rev. Lett.* **2002**, *89*, 227203
43 Yoshida, H.; Muraoka, Y.; Sörgel, T.; Jansen, M.; Hiroi, Z. *Phys. Rev. B* **2006**, *73*, 020408